NASA Contractor Report 195399

Characterization of Damage Progression in SCS-6/Timetal 21S $[0]_4$ Under Thermomechanical Fatigue Loadings

Michael G. Castelli
NYMA, Inc.
Engineering Services Division
Brook Park, Ohio

Prepared for the
Symposium on Life Prediction Methodology for Titanium Matrix Composites
sponsored by the American Society for Testing and Materials
Hilton Head, South Carolina, March 22–24, 1994

Prepared for
Lewis Research Center
Under Contract NAS3–27186

National Aeronautics and
Space Administration

CHARACTERIZATION OF DAMAGE PROGRESSION IN SCS-6/TIMETAL 21S $[0]_4$ UNDER THERMOMECHANICAL FATIGUE LOADINGS

Michael G. Castelli
NYMA, Inc.
Engineering Services Division
Brook Park, Ohio

ABSTRACT: A detailed experimental investigation was performed at a single maximum cyclic stress (σ_{max}) level to physically characterize the progression of thermomechanical fatigue (TMF) damage in continuously reinforced [0°] SCS-6/Timetal 21S, a titanium matrix composite. In-phase (IP) and out-of-phase (OP) loadings were investigated at σ_{max} = 1000 MPa with a temperature cycle from 150 to 650°C. Damage progression, in terms of macroscopic property degradation, was experimentally quantified through an advanced TMF test methodology which incorporates explicit measurements of the isothermal static moduli at the TMF temperature extremes and the coefficient of thermal expansion (CTE) as functions of the TMF cycles. Detailed characterization of the physical damage progression at the microstructural level was performed by interrupting multiple TMF tests at various stages of mechanical property degradation and analyzing the microstructure through extensive destructive metallography. Further, the extent of damage was also quantified through residual static strength measurements. Results indicated that damage initiation occurred very early in cyclic life ($N < 0.1N_f$) for both the IP and OP TMF loadings. IP TMF damage was found to be dominated by fiber breakage with a physical damage progression in the microstructure which was difficult to quantify. OP TMF loadings produced matrix cracking exclusively associated with surface initiations. Here, damage progression was easily distinguished in terms of both the number of cracks and their relative inward progressions toward the outer fiber rows with increased cycling. The point at which the leading cracks reached the outer fiber rows (when localized fiber/matrix de-bonding and matrix crack bridging occurred) appeared to be reflected in the macroscopic property degradation curves.

KEYWORDS: metal matrix composites, damage progression, thermomechanical fatigue, mechanical properties, stiffness, coefficient of thermal expansion.

Introduction

Silicon-carbon fiber reinforced titanium matrix composites (TMCs) have recently received considerable attention in the research community for potential use in advanced high temperature airframe and propulsion system applications. The obvious attractions of such materials are their relatively high stiffness and strength to weight ratios at elevated temperatures, when compared to monolithic materials. Studies aimed at experimentally characterizing the elevated temperature behavior of TMCs have revealed many of the complexities introduced by incorporating constituents with vastly differing mechanical properties. Many of these complexities, such as coefficient of thermal expansion (CTE) mismatch and matrix load shedding, are particularly highlighted under thermomechanical fatigue (TMF) conditions [1-10] where dominant damage mechanisms have been clearly shown to be functions of not only the load-temperature phasing, but also the multitude of additional environmental and mechanical test parameters.

If damage modeling for this class of materials is to be entirely successful under general TMF loading conditions, the fundamental mechanisms detailed in the cited studies must be represented. Experimental studies often discuss the TMF mechanisms in terms of the various observations made

through fractography and metallography on specimens cycled to failure. Though this information is extremely useful, it is often times only qualitative and lacks specific details concerning the physical progression of damage. To supplement this information, a recent advance in TMF testing was introduced to experimentally quantify TMF damage progression at the macroscopic property level [11]. This technique incorporated explicit measurements to track the degradations of the isothermal stiffness (E) and coefficient of thermal expansion (CTE) as functions of accumulated cycles, and has been found to provide unique insights to the nature and progression of TMF damage in TMCs [5-7,11]. By combining this information with that obtained from the microscopy, a further characterization is obtained; however, questions still persist concerning the physical damage progression at the microstructural level and its relative impact on the macroscopic mechanical properties. The study presented here was undertaken to address this concern.

The objective of this study was to mechanically and physically characterize the progression of damage in SCS-6/Timetal 21S $[0]_4$ under idealized thermomechanical fatigue (TMF) loading conditions at a single maximum cyclic stress (S_{max}) level. The general TMF deformation and life trends of this TMC are briefly reviewed from a previous study [5] with particular reference to the damage progression as gauged by the E and CTE degradation measurements. With this information, a series of specimens were cycled under identical TMF conditions at a S_{max} level of 1000 MPa to 10, 50 and 90 percent of the expected cyclic life under OP conditions and to an initial damage state and a mid-to-late damage state under IP conditions. At these various states of degradation, the specimens were subjected to destructive metallography to examine the extent of physical damage in the microstructure. Optical and scanning electron microscopy (SEM) were employed. Further, a second set of specimens was cycled in identical fashion for the OP TMF condition and tensile tested at room temperature to investigate residual strength properties. Results from these various progressive damage tests are discussed and interpreted in view of the macroscopic property degradation data.

Material and Test Details

The TMC used in this study was SCS-6/Timetal 21S[1] $[0]_4$. The SCS-6 is a SiC fiber (manufactured by Textron Specialty Materials) with a nominal diameter of 140 μm. Timetal 21S is a beta-phase titanium alloy with a nominal composition of Ti-15Mo-3Nb-3Al-0.2Si (weight percent). The TMC panel was fabricated by hot isostatic pressing alternate layers of Timetal 21S foil and SCS-6 fiber mat; TiNb ribbon was used for crossweave material in the fiber mats. The composite had a nominal fiber volume fraction of 0.33 and a nominal thickness of 1.0 mm. Coupon test specimens were cut from the panel using abrasive waterjet machining with no additional surface or edge preparation. All specimens were subjected to a pre-test heat treatment consisting of an 8 hour soak in vacuum at 621°C to stabilized the alpha plus beta titanium microstructure of the Timetal 21S. The coupon specimen design is a "dogbone" geometry featuring a length of 15.2 cm, a radius cut of 36.8 cm, and a central parallel section with a length and width of 26 and 10 mm, respectively. This design proved to be very successful at ensuring specimen failures within the stress and temperature controlled parallel section. Metal tabs were attached to the ends of the specimen to alleviate stress concentrations induced at the gripping locations.

All fatigue tests were conducted in air on a computer-controlled servo-hydraulic test system equipped with water-cooled grips. A triangular waveform was used for the load under load-controlled, zero-tension (max/min stress ratio = 0) conditions. In-phase (IP) and out-of-phase (OP) TMF loadings with S_{max} = 1000 MPa were examined with a cyclic frequency of 5.56×10^{-3} Hz (3 minute period) and a temperature cycle using a triangular waveform from 150 to 650°C. IP and OP loadings were defined as 0° and 180°, respectively, time phase shifts between the load and temperature waveforms. Axial strain measurements were made over a centrally located 12.7 mm gage length with a water-cooled

[1]Timetal 21S is a registered trademark of TIMET, Titanium Metals Corporation, Toronto, Ohio.

extensometer mounted on the edge of the specimen. Intrinsic K-type thermocouples were used for temperature monitoring and closed-loop control. The thermocouple locations did not exhibit premature cracking, and thus were considered to have had a negligible influence on the specimen fatigue life. Specimen fatigue life is defined as the number of cycles to failure (N_f) where failure represents complete separation of the specimen into two pieces. Tensile residual strength tests were conducted at room temperature in strain control with a tensile strain rate of $1.0x10^{-4}$ s^{-1}.

The TMF test technique used in this study [11] to experimentally quantify both the stiffness and the CTE degradations during TMF testing is shown graphically in Fig. 1. After each TMF cycle designated for data collection, the specimen was subjected to a thermal cycle under zero load, represented by the horizontal line from T_1 to T_2 at zero load. This thermal cycle allowed the real-time or "current" thermal strain properties of the composite to be explicitly measured with the extensometer. At the extremes of the thermal cycle (i.e., 150 and 650°C), the temperatures were briefly stabilized and small "elastic" loads were applied; these loadings are represented by the stress-strain lines in Fig. 1 with slopes marked E_1 and E_2. This allowed explicit measurement of the "current" isothermal material stiffness at both temperature extremes. Note that the E measurements are essentially a Young's modulus measurement (see ASTM Standard E111), from zero macroscopic load. The maximum stress levels used to obtain E were kept relatively small (80 MPa) to facilitate a non-damaging, linear-elastic response.

In comparison to an uninterrupted "conventional" TMF test, this technique introduced several additional thermal cycles at zero load and several relatively small elastic loads. These additional loadings were found to be inconsequential with respect to the ongoing material damage and resulting TMF life at the stress levels investigated. This was verified throughout the development and implementation of the test technique [11].

One advantage of this test methodology was the ability to record the "real-time" thermal strain information, which was essential for accurate post-test assessment of the mechanical strain response (total minus thermal strain) [5-7,11]. Also, and most critical to the present work, the CTE and isothermal E measurements provided definitive, quantitative means for tracking the TMF damage progression in terms of macroscopic property degradation.

Results and Discussion

Deformation and Life

Prior to discussing the TMF damage progression, it is worthwhile to briefly review the general TMF deformation and life exhibited by this TMC [5]. Representative deformation behaviors for OP and IP TMF with S_{max} = 1000 MPa are shown in Fig. 2, where maximum cyclic mechanical strain values are plotted. As indicated, OP TMF loadings did not promote excessive strain ratchetting, as the OP S_{max} occurs at T_{min} (150°C) where matrix load shedding due to time dependent deformation and tensile strain ratchetting was minor. Further, the maximum strain increases illustrated in Fig. 2 which occurred later in TMF life will be shown to have resulted primarily from increases in composite compliance (stiffness degradation). In contrast, IP load controlled TMF conditions were highly conducive to strain ratchetting, indicated in Fig. 2 by the large maximum mechanical strain increases early in cyclic life. Here, S_{max} and T_{max} loadings coincide, promoting matrix load shedding due to time dependent deformation, as seen in previous TMF experimental studies on [0] TMCs [1-5] and modeled through various time-dependent and viscoplastic analyses [12-15]. Subsequent discussions of the stiffness degradations under IP conditions will show that the majority of mechanical strain increase is associated with strain ratchetting rather than an increase in composite compliance.

TMF life results for SCS-6/Timetal 21S $[0]_4$ are plotted in Fig. 3. In general, IP TMF loading conditions were found to be life-limiting under relatively high S_{max} conditions where the strain ratchetting mechanisms mentioned above led to excessive strains. The IP and OP TMF life trends crossed at a S_{max} of approximately 1000 MPa, below which OP conditions resulted in shorter cyclic lives. Based on these TMF life trends, a S_{max} of 1000 MPa was chosen for the present study, so as to

investigate the damage progression under IP and OP conditions resulting in comparable lives. This selection also served to equalize temperature exposure times and thus, the potential for environmental degradation.

Macroscopic Property Degradation

Out-Of-Phase TMF

As previously stated, the TMF test technique used in this study explicitly measured isothermal E and CTE as functions of accumulated TMF cycles; these data are shown in Figs. 4a and 4b, respectively, for the OP TMF test with S_{max} = 1000 MPa. Note that the isothermal E measurements for this one test are represented in Fig. 4a by two sets of data consisting of the isothermal E values measured at the temperature extremes of the TMF cycle, that is, E_{150} and E_{650}. The dashed vertical lines on the graphs represent points at which progressive damage tests were interrupted and destructively examined; subsequently discussed.

Several noteworthy trends were evident in Fig. 4a concerning the E degradations. First, the E values measured from the OP test did not degrade equally, but rather, the E_{150} ultimately degraded much more severely, even to the point where the E_{150} and E_{650} were essentially equal just prior to failure (that is, in a highly damaged state). Previous studies [1-5] have shown that the dominant damage mechanisms in [0] TMCs under OP TMF loadings was matrix damage in association with minimal fiber cracking. Using a simple rule of mixtures approach to composite stiffness, one notes that the contribution of the matrix is much greater at 150°C than at 650°C. This comes from the fact that the stiffness of the Timetal 21S matrix is strongly dependent upon temperature in this temperature range [16]; see Table 1. Given this fact, and considering a continual degradation of the effective matrix contribution in the presence of undamaged fibers, the relative degradation of the composite E_{150} values will be greater than that experienced by the composite E_{650} values. Further, in a case where the matrix approaches a "completely" damaged state, the composite E values at both temperature extremes will degrade to similar quantities, given that the SCS-6 fiber stiffness is relatively insensitive to temperature over this temperature range [17]; see Table 1. For example, using the values provided in Table 1, the composite stiffnesses as calculated based solely upon the un-damaged fiber contribution are 128 and 122 GPa at 150 and 650°C, respectively.

It is important to note, however, that other factors, such as constituent stresses existing at zero macroscopic load, can influence this composite stiffness measurement and complicate a rule-of-mixtures interpretation. For example, subsequent to the matrix stress relaxation promoted during elevated temperature fatigue cycling, longitudinal matrix stresses induced by the fiber/matrix CTE mismatch can be compressive at relatively high temperatures and tensile at lower temperatures, all at zero macroscopic load. Such behavior can allow for closure of the matrix cracks at higher temperatures and crack opening at lower temperatures. Given the definition used for the composite stiffness, that is, the initial stress-strain slope from zero macroscopic load, it becomes apparent that a low temperature static stiffness measurement can actually fall below that measured at a higher temperature (by inducing matrix crack closure at the higher temperature); see [5] for a case in point.

Degradation of the CTE of the TMC during OP TMF with S_{max} = 1000 MPa is shown in Fig. 4b. This macroscopic property can be tracked either in terms of an instantaneous value at a given temperature, or a mean value between two temperatures. The latter approach is taken here for ease of discussion. The mean CTE was calculated by taking the thermal strain range, as measured under zero macroscopic load, from 150 to 650°C and dividing it by ΔT, that is, 500°C. Thus, it represents the average CTE for the TMF temperature cycle.

As shown in Figure 4b, the macroscopic mean CTE of the TMC is essentially constant up to approximately $\frac{1}{2}N_f$. Subsequently, the property degrades a relatively small degree to a total degradation of approximately 5 percent prior to failure. Previous experimental studies where CTE degradation was monitored has shown this measurement to be a good indicator of matrix dominated damage, particularly at relatively low S_{max} levels where matrix crack growth can mature and dominate

the cross-section prior to overload failure [5-7]. In such cases, the degradation of this property has been observed to be as high as 25 percent. It is important to point out that this macroscopic property not only changes with damage, but has also been shown in other metal matrix composites to change with inelasticity of the matrix, and constituent stress redistributions [18]. However, the stiffness measurements discussed above clearly suggest the progression of damage.

In Phase TMF

In similar fashion to that of Figs. 4a and 4b, Figs. 5a and 5b contain the isothermal E and CTE degradation curves, respectively, for an IP TMF test with S_{max} = 1000 MPa. Fig. 5a reveals that the IP TMF damage promoted a relatively small, but detectable stiffness degradation. In contrast to the OP TMF degradation, the magnitude of degradation was comparable at both temperature extremes. This change is often not obvious from the deformation data, as a clear assessment of stiffness/compliance is somewhat convoluted because of the strain ratchetting, continually changing temperature, and potentially changing thermal strain component [5, 11]. Again, using a simple rule of mixtures interpretation and recalling from previous studies that typical IP TMF damage was dominated by fiber cracking [1-5], it is easily shown that a reduction of the effective SCS-6 contribution to the composite stiffness will promote reductions of comparable magnitudes in this measurement at 150 and 650°C because the SCS-6 fiber stiffness is relatively insensitive to temperature over this range. This may not suggest that the fiber stiffness is actually decreasing, but rather that the *effective fiber contribution* to the composite stiffness is decreasing. This effect may be a result of the fiber cracking and highly localized de-bonding associated with the crack locations. The data also reveals that the stiffness degradation occurred very early in cyclic life where strain ratchetting is most severe, and tended to stabilize after approximately 100 cycles.

Degradation of the TMC CTE during IP TMF is shown in Fig. 5b. As seen in this figure, the TMC experiences only a small decrease in mean CTE with S_{max} = 1000 MPa IP TMF cycling, as the total change represents a change in thermal strain range of approximately 100 μm/m. Note, however, the similarity in trends with the stiffness degradation and strain ratchetting, as the majority of change occurs early in cyclic life.

Evolution of Microstructural Damage Under OP Conditions

10 percent N_f - The first stage of microstructural damage investigated was that at 10 percent N_f for the OP TMF condition discussed in Figs. 2 and 4. Shown in Fig. 6 is a metallographic section taken from a specimen interrupted at this level; the cut is a longitudinal section through the thickness (LST) with the micrograph revealing the surface edge of the specimen. As seen here, OP TMF conditions produced very fine surface initiated matrix cracks at this early stage in TMF life. Individual cracks were relatively numerous throughout the gage section and exhibited an average length into the specimen thickness of 10 to 20 μm. As shown in Fig. 7, this early stage of matrix cracking was readily detectible on the specimen surface through the use of SEM. Here, numerous cracks were found predominantly transverse to the loading direction with lengths across the specimen width as great as 80 μm. It is noteworthy to state that the majority of initiation points detected were found to be associated with "rough" surface features (Recall that specimens were tested with as-received surface conditions, as typical of most TMC testing to date.). As would be expected with most metallic materials, this suggests that surface polishing may extend the time to crack initiation. It is apparent that the slight degradation detected in Fig. 4a by the E_{150} measurements are indications of these very early surface initiations. Again, the fact that the E_{150} measurements detected this damage and the E_{650} measurements did not, is likely related to the respective matrix stress states at the two temperatures (discussed above).

Additional longitudinal sections through the width (LSW) and transverse sections (TS) did not reveal any further degradation in either of the constituents with one exception; highly localized

fiber/matrix (F/M) de-bonds were evident at the TiNb crossweave locations, such as that pictured in Fig. 8 where the weave appears as a white "band" in the matrix, subsequent to a lactic acid etch. Although this effect was present at this 10 percent stage and all subsequent damage states examined, it did not appear to preferentially initiate or enhance matrix cracking.

50 percent N_f - The next damage state examined was that existing after the specimen was cycled to 50 percent N_f. Here, the OP specimen revealed an orderly progression of matrix cracking. The surface initiated matrix cracks were now found to have propagated an average distance of 60 μm into the specimen thickness with a maximum visible penetration of approximately 100 μm. Nowhere was it apparent that the major cracks had reached the outer most fiber rows (subsequently referred to as the first fiber rows), as the outer surface of the fiber was approximately 130 μm from the surface. Initial stages of crack branching were visible in the LST mount (shown later in the $0.9N_f$ damage state) but it was visible on only a relatively small number of the larger cracks. On the specimen surface, individual cracks were still predominantly transverse to the loading, but at this stage, the lengths across the specimen width were on average 200 μm.

LSW and TS mounts confirmed that at this damage state, the cracks had not reached the first fiber rows, as no F/M de-bonding was apparent. Also, no fiber cracking was visible. Note from the E_{150} (Fig. 4a) and the CTE (Fig. 4b) degradation curves that slope decreases (increased degradation rates) occurred after approximately cycle 400, which was slightly after this interrupt point. From the microstructural evidence available, this was likely the point at which the major cracks reached the first fiber rows, as this would introduce an additional damage component, namely, F/M de-bonding. Prior to this event, however, it is not clear as to why the CTE did not reveal some degradation associated with the matrix cracking.

90 percent N_f - The last OP specimen examined was interrupted at the 90 percent N_f level, as indicated again by the dashed line on Fig. 4. The microstructural damage was now quite extensive, with the most obvious progression being that the cracks had reached and propagated just beyond the first fiber rows. Many of the larger cracks exhibited extensive branching such as that illustrated in the LST mount shown in Fig. 9. Also shown in this figure was the de-bonding at the F/M interface which was, at this stage, common to the vast majority of fibers in the first fiber rows. This effect was most evident in the LSW mounts revealing one of the outer most fiber rows, such as that illustrated in Fig. 10. Here, substantial matrix cracking, F/M de-bonding, and crack bridging were all apparent. Even at this extensive state of damage, no fiber cracking was identified. A surface view of the matrix cracks revealed transverse lengths (across the specimen width) of up to 400 μm. At this 90 percent N_f level, both the E and CTE degradations were distinct, indicating the severe damage revealed in the microstructure. One effect which was not quantified in this study or mentioned thus far, but was clearly found to play a role in the failure mechanisms was environmental degradation. Failure surfaces from the TMF life study [5] revealed strong environmental interaction, as all matrix cracks were found to be heavily oxidized. A previous study designed to isolate the environmental degradation effects under TMF conditions revealed a dramatic impact on resulting OP TMF lives [3]. Thus, it is sufficient to state that all of the OP damage mechanisms discussed were enhanced by the oxidizing environment.

Residual Strength Under OP Conditions

In addition to the characterization of microstructural damage progression, room temperature tensile residual strengths were also examined to assist in quantifying the damage states. These tests were conducted after the specimens were subjected to the various percentages of OP TMF life with S_{max} = 1000 MPa. Shown in Fig. 11 are the results from the tensile residual strength measurements. At 10 percent of the expected N_f, reductions of 7 and 9 percent were realized in the ultimate tensile strength (S_{ult}) and strain to failure (e_f), respectively. Little or no reduction in room temperature E was

detectable, as consistent with the E degradation curves given in Fig. 4a. After 350 cycles of OP TMF (50 percent N_f), the tensile response revealed clear signs of the matrix damage discussed above. With only a nominal reduction evident in the room temperature E, significant reductions of 18 and 22 percent were found to occur in the S_{ult} and e_f, respectively. Though the e_f remains moderate for this TMC, one can see that the onset of non-linearity occurs much earlier as a result of the matrix cracks which were relatively close to the first fiber rows at this stage of TMF damage.

The final stage of damage investigated, 90 percent N_f, reveals a dramatic change in tensile behavior, as reductions of 40 and 45 percent were realized in the S_{ult} and e_f, respectively. Note the essentially linear behavior to complete failure. Recall that at this damage state, the matrix cracks had propagated from the surface to just beyond the first fiber rows, but the fibers appeared to be intact, beyond obvious damage to the outer carbon coatings. If a rule-of-mixtures calculation of S_{ult} is made (which is reasonably accurate for the un-fatigued sample with S_{ult} of the fiber = 4000 MPa and S_{ult} of the Timetal 21S = 1100 MPa) assuming no matrix contribution, the result is 1320 MPa. This implies that the composite strength at this stage of damage is less than the "fiber only" strength and suggests that some degree of fiber strength degradation is present, especially in light of the fact that the micrographs from above do not show the matrix to be "fully damaged". This loss in fiber strength could result from a number of effects, including environmental degradation, the carbon coating damage cited above, and appropriate stress concentrations resulting from the matrix cracks.

To summarize the degradation of the room temperature residual strength tensile properties, the stiffness, ultimate strength, and strain to failure are plotted in Fig. 12 as normalized values with respect to the properties obtained from the un-fatigued sample. It is interesting to note that a straight line approximates the residual strength property data with reasonable accuracy.

Evolution of Microstructural Damage Under IP Conditions

An investigation similar to that discussed above for the OP condition was attempted for S_{max} = 1000 MPa under IP loadings. Unfortunately, the IP TMF damage progression and lives proved to be much less deterministic in nature. Thus, in the process of obtaining the 50 and 90 percent N_f specimens based upon the S_{max} = 1000 MPa TMF life illustrated in Figs. 2 and 5, "premature" specimen failures were realized. These life points are also plotted in Fig. 3. This was the case, even though the property degradation patterns were similar for each of the specimens. Note again that the vast majority of property degradation occurred very early in the TMF life. As a result of the non-deterministic failure experienced under the IP condition, it was not possible to state with sufficient confidence that a particular specimen was at a given percentage of expected life (given that N_f was found to vary from 90 to 647 cycles). However, it was worthwhile to consider the evolution of microstructural damage at both a relatively early stage in the TMF life and at a later stage, even if this state could not be explicitly quantified in terms of cyclic life. Thus, the following microstructural examination will address these two states.

Initial Damage State - Similar to the OP specimen which revealed microstructural damage after experiencing only 70 cycles (10 percent N_f) with S_{max} = 1000 MPa, the specimen subjected to 65 cycles of IP loading also revealed physical damage at this early stage. This damage was fiber cracking. Fiber cracking, such as that shown by the LSW mount in Fig. 13, was evident in multiple fibers; however, many fibers did not exhibit cracking. The cracks were relatively fine and most often found only in the Si rich "outer" portion of the fiber and did not appear to continue through the fiber's carbon core. Although some degree of highly localized F/M de-bonding was likely associated with the fiber crack locations, it was not clearly visible on the metallographic mounts. This physical identification of fiber cracking very early in cyclic life is consistent with a similar TMF study by Neu and Roman [19] where acoustic emission (AE) indications suggested numerous fiber breakage events on the first IP TMF cycle at this S_{max} with a slightly higher fiber volume ratio.

As found in the OP specimen examined at 10 percent N_f, the initial damage state under IP conditions also revealed highly localized fiber/matrix (F/M) de-bonds at the TiNb crossweave

locations, similar to that illustrated in Fig. 8. Again, although this effect was present at this early stage of damage and in the latter stage examined, it did not appear to enhance or preferentially initiate the fiber cracks. Additional LSW, LST, TS mounts did not reveal any matrix cracking or further degradation in either of the constituents.

Mid-to-Late Damage State - In contrast to the OP damage progression, the IP TMF test interrupted at the mid-to-late damage state did not reveal a clear progression of damage from that evident at the earlier damage state. Subsequent to 325 IP TMF cycles, only a slight increase in fiber cracking was apparent. Transverse cracks were again evident in many of the fibers; however, each of the sections also revealed fibers which appeared un-cracked. One feature which potentially did increase was the amount of visible "v-wedge" cracks, termed so because of their appearance in the plain exposed by a LSW mount, as shown in Fig. 14 on the four right-most fibers. This 2-dimensional view may be suggesting a 3-dimensional spiral-type crack path about the carbon core. F/M interface de-bonding at the fiber crack locations remains difficult to detect. Further, many cracks in the Si rich region of the SCS-6 fiber appear to stop (or begin) at the innermost carbon coating on the outside diameter of the fiber, with the outermost carbon coating appearing to be intact. Note, however, that this observation is subject to the various 2-dimensional views enabled by the metallographic mounts. (See [20] for a complete description of the SCS-6 fiber and its various microstructural features.)

In comparison to the observations made from the initial damage state, it can be suggested with only a small degree of confidence that at this mid-to-late damage state *i*) the fiber cracks are more numerous, *ii*) the un-broken fiber lengths between cracks are on average smaller, and *iii*) the axial fiber crack openings are slightly larger. For these observations to be confirmed with even modest quantitative significance, it is apparent that a more comprehensive study involving multiple specimens and mounts at each damage state would likely be necessary. It can be said, however, that even at this mid-to-late stage of damage progression no matrix cracking could be identified on any of the mounts. Recalling the macroscopic property trends established in Fig. 5, one notes that very little additional stiffness degradation was detected beyond that which existed early in cyclic life, and only a relatively small CTE degradation could be measured. In contrast to what the data appeared to suggest here, it is noteworthy to state that the previously cited study [19] which utilized AE to detect fiber breaks, strongly suggested that additional fiber breaks occurred with continued IP TMF cycling in this life regime.

Residual strength measurements of specimens subjected to IP TMF cycling were not available for this report.

Summary/Conclusions

A detailed experimental investigation was conducted at a single maximum cyclic stress level (S_{max} = 1000 MPa) to characterize the thermomechanical fatigue (TMF) damage progression in SCS-6/Timetal 21S $[0]_4$ under in-phase (IP) and out-of-phase (OP) loading conditions with a temperature cycle from 150 to 650°C. The progression of damage was characterized at the macroscopic level through explicit measurements of the composite isothermal static moduli (E) and coefficient of thermal expansion (CTE). The progression of damage at the microstructural level was characterized through a systematic series of tests interrupted at various percentages of expected cyclic life (N_f) and then destructively prepared for examination using optical and scanning electron microscopy. In addition, OP TMF damage was further quantified through residual static strength measurements on specimens cycled to various percentages of expected life. Results from this study have indicated the following:

Out-of-Phase Damage Progression

- Initiation of damage occurs very early in cyclic life, as multiple surface initiated matrix cracks were found approximately 20 to 40 μm into the specimen thickness at $0.1N_f$. A modest drop

of less than 10 percent was realized in the room temperature ultimate tensile strength (S_{ult}) and strain to failure (e_f).

- At $0.5N_f$, surface initiated cracks were observed to have propagated at most a length of 100 μm into the specimen thickness, approximately 30 μm away from the outer most fibers. Initial crack branching was evident in the major cracks. No fiber cracking was apparent. Measurements of E at 150°C clearly indicated the presence of damage, but macroscopic CTE measurements revealed no change. Room temperature residual strength properties dropped by approximately 20 percent.
- At $0.9N_f$, numerous matrix cracks had reached and propagated slightly beyond the first rows of fibers causing considerable fiber/matrix (F/M) de-bonding. Extensive matrix crack branching was evident, but fiber cracking remained undetectable. The E_{150} values had degraded by 13 percent and were approximately equal in magnitude to those measured at 650°C. CTE measurements also revealed a modest degradation. Room temperature residual strength properties were degraded by more than 40 percent, with S_{ult} = 1230 MPa and e_f = 0.0067 m/m.

In-Phase Damage Progression

- Initiation of damage occurs very early in cyclic life, as numerous, relatively fine fiber cracks were identified. Macroscopic E and CTE measurements revealed small, but measurable degradations on the order of 3 to 5 percent with trends coincidental to those of the strain ratchetting.
- At mid-to-late stages of cyclic life, the microstructural damage progression could not be clearly distinguished. Fiber/matrix de-bonding at the cracked fiber locations remained difficult to detect. No matrix damage was visible. The E measurements did not reveal any further degradation and the CTE values revealed only a slight decrease.
- The non-deterministic IP failures observed in this investigation suggested that a more comprehensive study involving multiple specimens and mounts at each damage state would likely be necessary to appropriately quantify the microstructural damage progression.

Acknowledgements

Thanks be to God. The author also wishes to acknowledge Rod Ellis for his support and input to this research, and Chris Burke and Ralph Corner for their technical assistance in the Fatigue and Structures Laboratory and the Metallographic Laboratory at NASA Lewis Research Center.

References

1. Castelli, M.G., Bartolotta, P.A. and Ellis, J.R., "Thermomechanical Testing of High-Temperature Composites: Thermomechanical Fatigue Behavior of SiC(SCS-6)/Ti-15-3," Composite Materials: Testing and Design (Tenth Volume), ASTM STP 1120, Glen C. Grimes, Ed., Philadelphia, 1992, pp. 70-86.
2. Russ, S.M., Nicholas, T., Bates, M. and Mall, S., "Thermomechanical Fatigue of SiC/Ti-24Al-11Nb Metal Matrix Composites," Failure Mechanisms in High Temperature Composite Materials, AD-Vol. 22 and AMD-Vol. 122, Eds. G.K. Haritos, G. Newaz and S. Mall, ASME, New York, 1991, pp. 37-43.
3. Bartolotta, P.A., Kantzos, P., Verrilli, M.J. and Dickerson, R.M., "Environmental Degradation of an Intermetallic Composite During Thermomechanical Fatigue," Fatigue 93, Vol. 2, Eds. J.P. Bailon and J.I. Dickson, 1993, pp. 1001-1006.
4. Neu, R.W. and Nicholas, T. Effect of Laminate Orientation on the Thermomechanical Fatigue Behavior of Titanium Matrix Composites. J. of Composites Technology and Research, Vol 16, No. 3, July, 1994, pp. 214-224.
5. Castelli, M.G., "Thermomechanical Fatigue Deformation, Damage and Life of SCS-6/Timetal 21S $[0]_4$," International Journal of Fatigue (submitted for publication).

6. Castelli, M.G., "Thermomechanical Fatigue Damage/Failure Mechanisms in SCS-6/Timetal 21S $[0/90]_s$ Composite," Composites Engineering, Vol 4, No. 9, 1994, PP. 931-946.
7. Castelli, M.G., "Thermomechanical and Isothermal Fatigue Behavior of a $[90]_8$ Titanium Matrix Composite," In: Proceedings of The American Society for Composites 8th Technical Conference on Composite Materials, Mechanics, and Processing, Oct., 1993, pp. 884-892, Technomic Pub. Lancaster, PA.
8. Majumdar, B.S. and Newaz, G.M., "Thermomechanical Fatigue of a Quasi-Isotropic Metal Matrix Composite," Composite Materials: Fatigue and Fracture (Third Volume), ASTM STP 1110, T. Kevin O'Brien, Ed., Philadelphia, 1991, pp. 732-752.
9. Johnson, W.S., Mirdamadi, M. and Bahei-El-Din, Y.A, "Stress-Strain Analysis of a $[0/90]_{2s}$ Titanium Matrix Laminate Subjected to a Generic Hypersonic Flight Profile," Journal of Composites Technology and Research, Vol. 15, No.4, Winter 1993, pp. 297-303.
10. Mall, S., Hanson, D.G., Nicholas, T. and Russ, S.M. Thermomechanical Fatigue Behavior of a Cross-Ply SCS-6/ß21-S Metal Matrix Composite. Constitutive Behavior of High Temperature Composites, MD-Vol. 40, B.S. Majumdar, G.M. Newaz and S. Mall, Eds. ASME, 1992, pp. 91-106.
11. Castelli, M.G., "An Advanced Test Technique to Quantify Thermomechanical Fatigue Damage Accumulation in Composite Materials," J. of Composites Technology and Research, Vol 16, No. 4, October, 1994.
12. Mirdamadi, M., Johnson, W.S., Bahei-El-Din, Y.A. and Castelli, M.G., "Thermal Mechanical Fatigue of Titanium Metal Matrix Composites Literature Review and Analysis," Composite Materials: Fatigue and Fracture, Fourth Volume, ASTM STP 1156, W.W. Stinchcomb and N.E. Ashbaugh, Eds., American Society for Testing and Materials, Philadelphia, 1993, pp. 591-607.
13. Neu, R.W. and Nicholas, T., "Thermomechanical Fatigue of SCS-6/TIMETAL 21S Under Out-of-Phase Loading," Thermomechanical Behavior of Advanced Structural Materials, W. F. Jones, Ed., AD-Vol. 34/AMD-Vol. 173, ASME, 1993, pp. 97-111.
14. Neu, R. W., "A Mechanistic-based Thermomechanical Fatigue Life Prediction Model for Metal Matrix Composites," Fatigue and Fracture of Engineering Materials and Structures, Vol. 16, No. 8, 1993, pp. 811-828.
15. Chamis, C.C., Tong, M.T. and Murthy, P.L.N., "Computational Simulation of Time-Dependent Behavior in Metal Matrix Composites Using METCAN," HITEMP Review 1992: Advanced High Temperature Engine Materials Technology Program, Vol. II, NASA Report CP-10104, NASA Lewis Research Center, Cleveland, OH, Oct., 1992, pp. 43:1-10.
16. Castelli, M.G., Arnold, S.M. and Saleeb, A.F., "Specialized Deformation Tests for the Characterization of a Viscoplastic Model: Application to a Titanium Alloy," NASA Report TM-106268, NASA Lewis Research Center, Cleveland, OH, 1994.
17. Textron Specialty Materials Data Sheet, Silicon Carbide Composite Materials, Lowell, Massachusetts.
18. Urguhart, E., Arnold, S.M., Pindera, M.J. and Aikin, B.J., "Simulation of Experimentally Observed Thermal Expansion Behavior of FeCrAlY-Based Composites," HITEMP Review 1993: Advanced High Temperature Engine Materials Technology Program, Vol. II, NASA Report CP-19117, NASA Lewis Research Center, Cleveland, OH, Oct., 1993, pp. 54:1-12.
19. Neu, R.W. and Roman, I., "Acoustic Emission Monitoring of Damage in Metal Matrix Composites Subjected to Thermomechanical Fatigue," Composites Science and Technology, submitted for publication.
20. Ning, X.J. and Pirouz, P., "The microstructure of SCS-6 SiC fiber," J. of Materials Res., Vol. 6, No. 10, Oct. 1991, pp. 2234-2248.

Temperature (°C)	SCS-6 Fiber (GPa)	Timetal 21S (GPa)
150	388	110
650	370	60 to 75[§]
	ΔE = 18	ΔE = 35 to 50

[§]This property exhibits a positive strain rate dependence.

Table 1. Static stiffness values for the SCS-6 fiber [17] and Timetal 21S foil matrix [16].

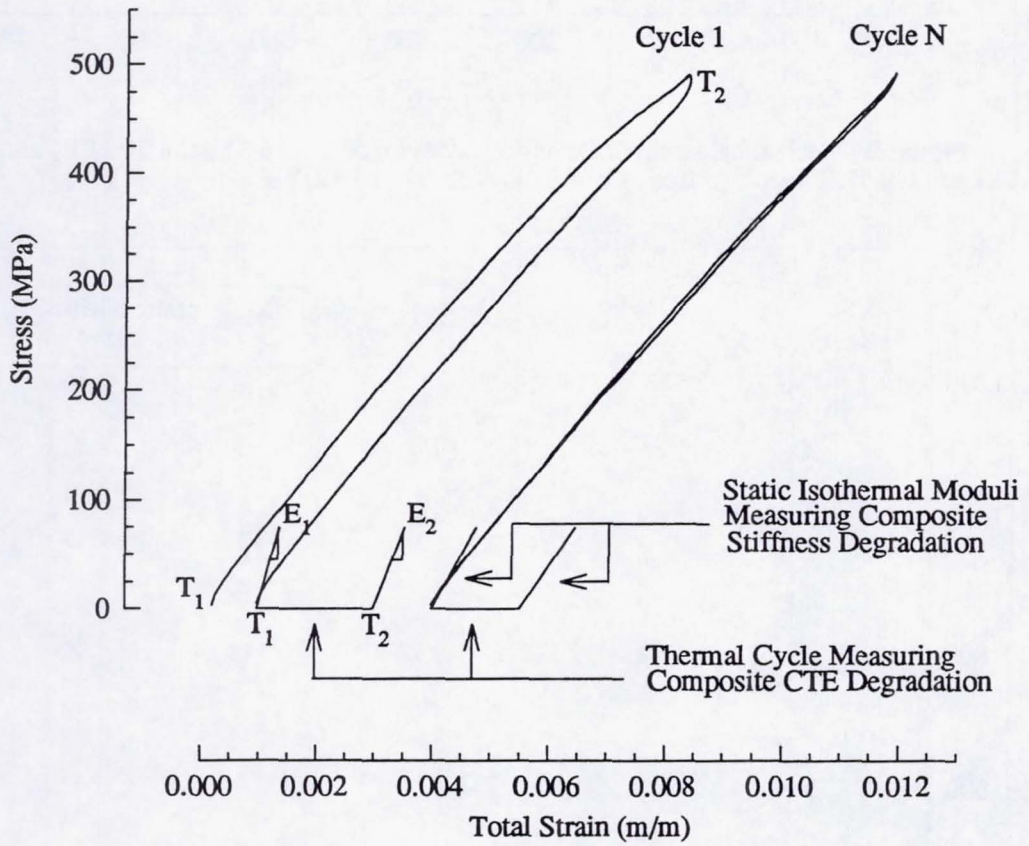

Figure 1. Advanced test technique enabling explicit measurement of the isothermal static moduli and CTE during TMF testing.

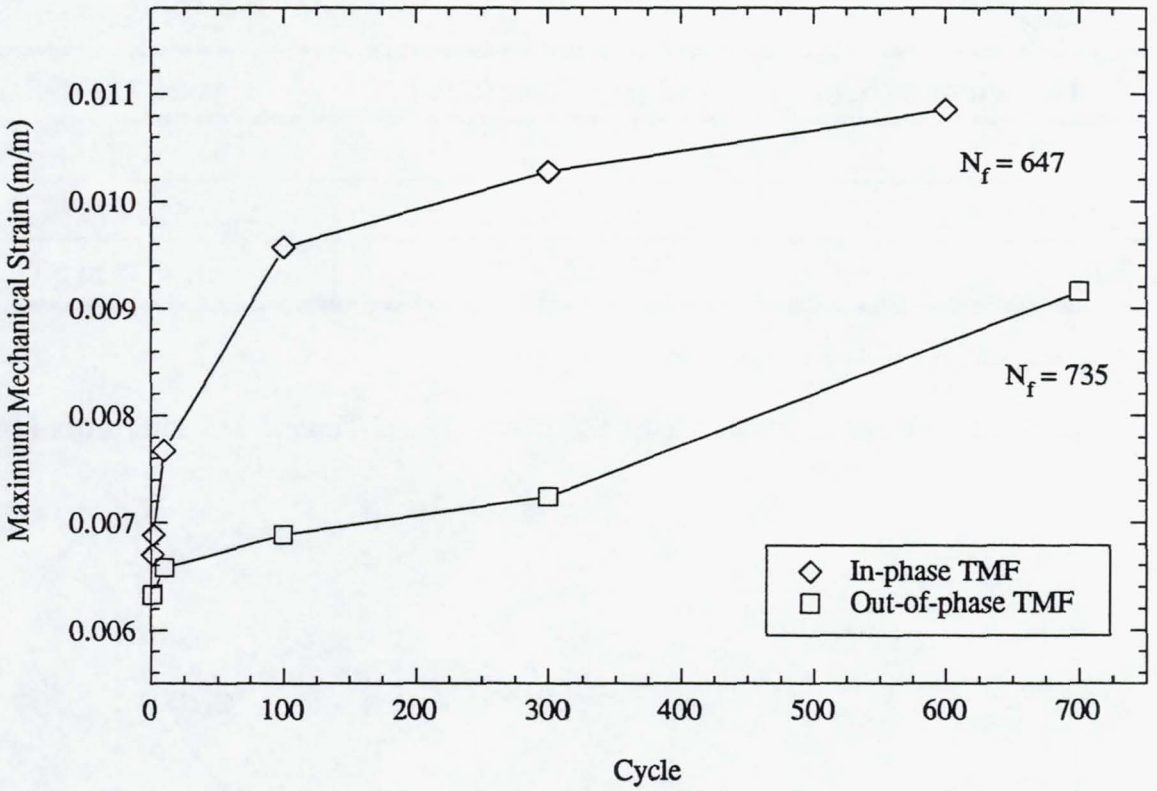

Figure 2. Mechanical strain deformation behavior of SCS-6/Timetal 21S $[0]_4$ under IP and OP TMF loadings from 150-650°C with S_{max}=1000 MPa.

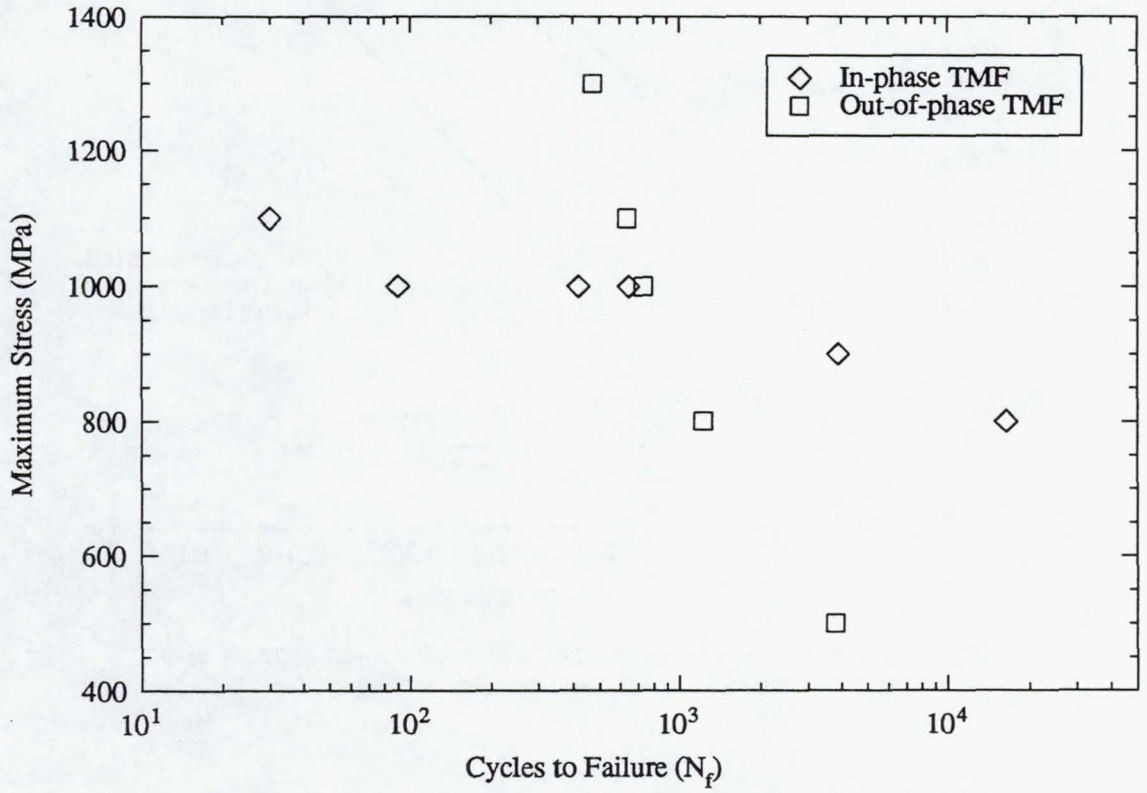

Figure 3. TMF life behavior of SCS-6/Timetal 21S $[0]_4$ under IP and OP loadings from 150-650°C.

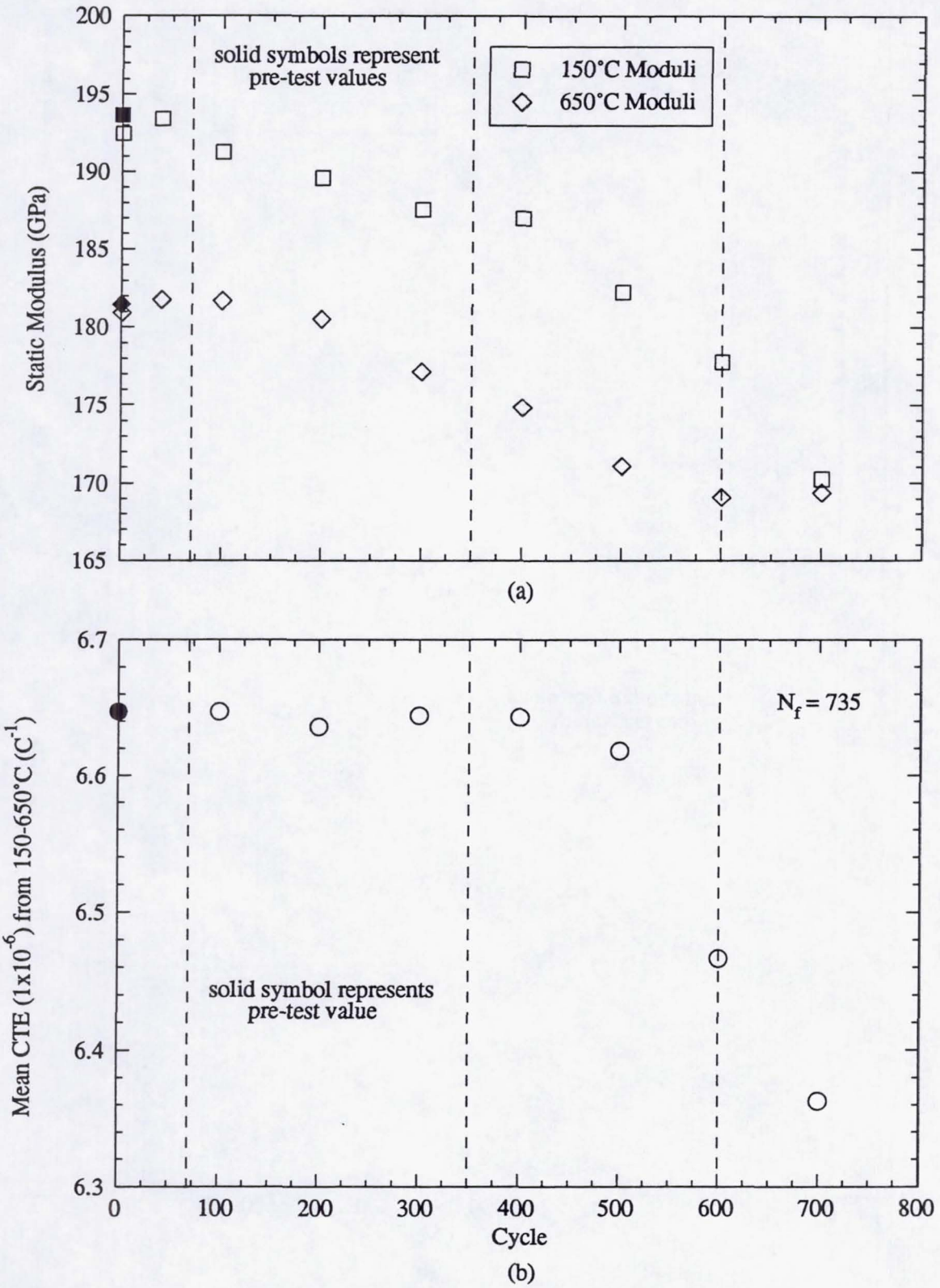

Figure 4. Thermomechanical fatigue degradation of the (a) isothermal moduli and (b) mean CTE under OP conditions with S_{max} = 1000 MPa.

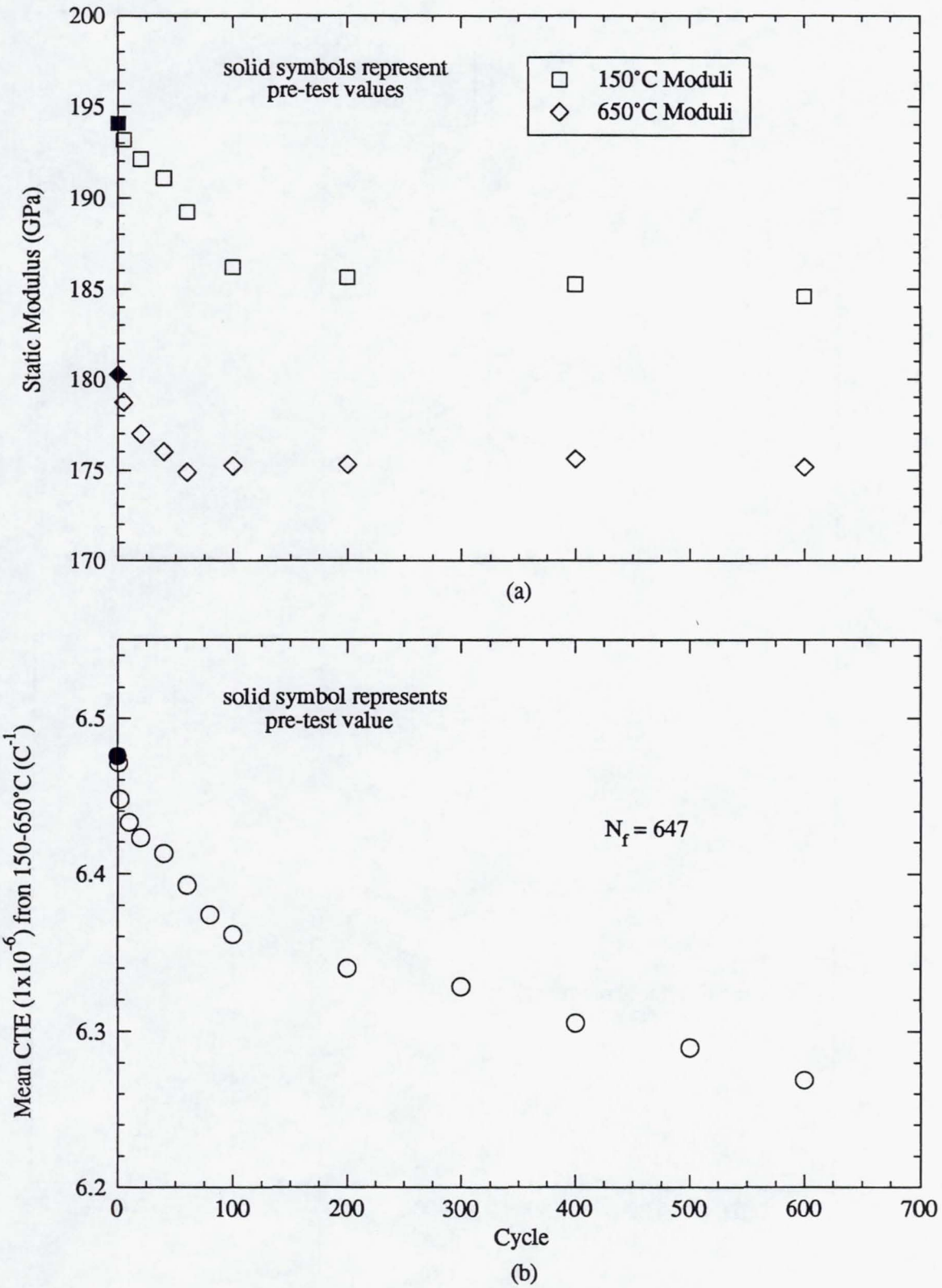

Figure 5. Thermomechanical fatigue degradation of the (a) isothermal moduli and (b) mean CTE under IP conditions with S_{max} = 1000 MPa.

Longitudinal Section into Specimen Thickness

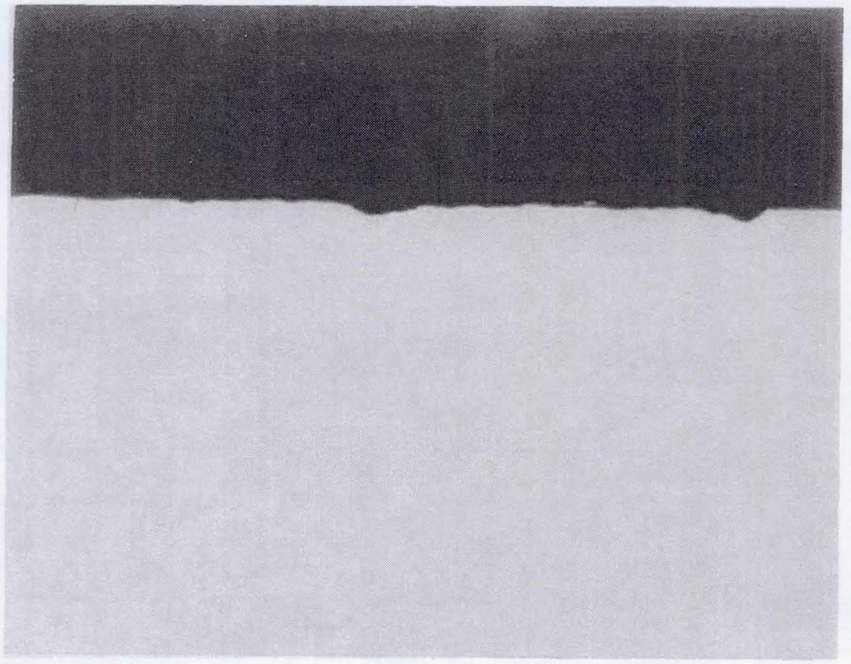

⟷ Loading Direction 20 μm

Figure 6. OP TMF damage progression at 10 percent N_f revealing surface initiated matrix cracks.

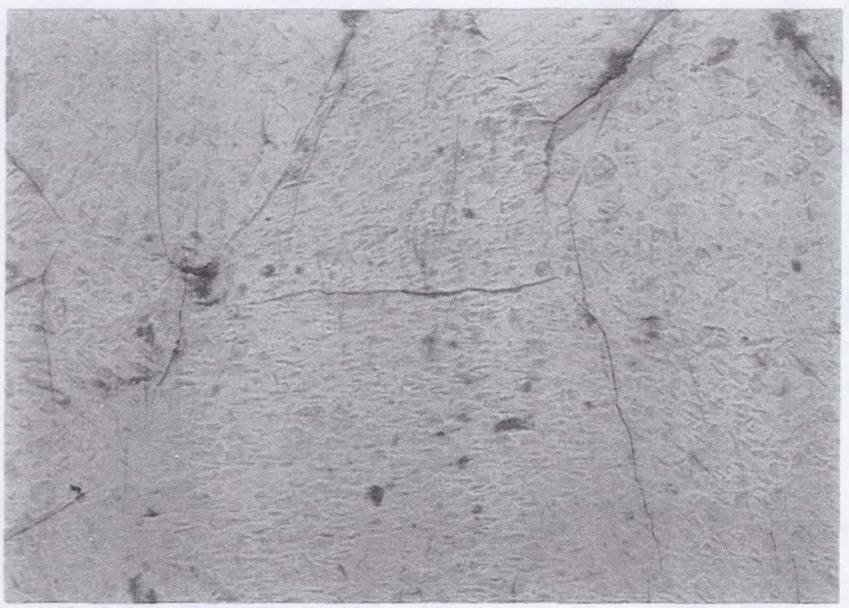

⟷ Loading Direction 25 μm

Figure 7. SEM of specimen surface revealing matrix cracks under OP TMF conditions at 10 percent N_f.

Longitudinal Section into Specimen Width

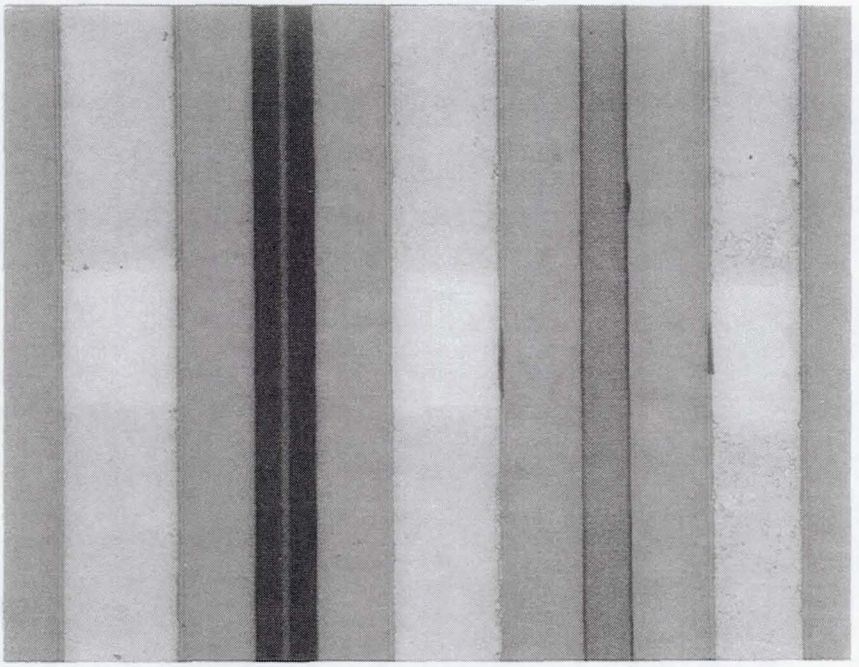

50 μm

Figure 8. Highly localized de-bonds evident at the 10 percent N_f OP TMF condition (shown) and the initial damage state IP TMF condition.

Longitudinal Section into Specimen Thickness

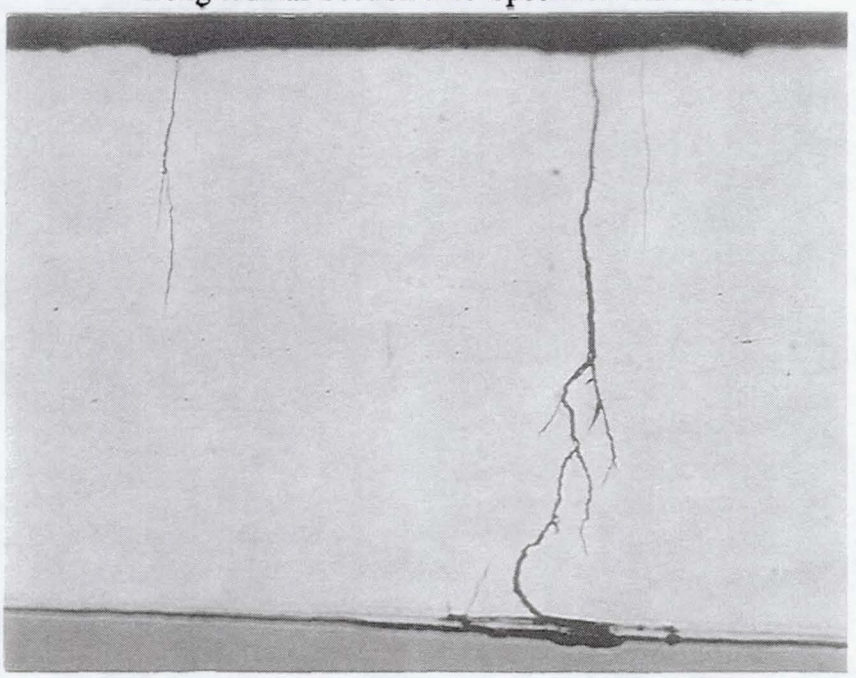

20 μm

Figure 9. OP TMF damage progression at 90 percent N_f revealing extensive matrix crack branching and F/M de-bonding at first fiber row.

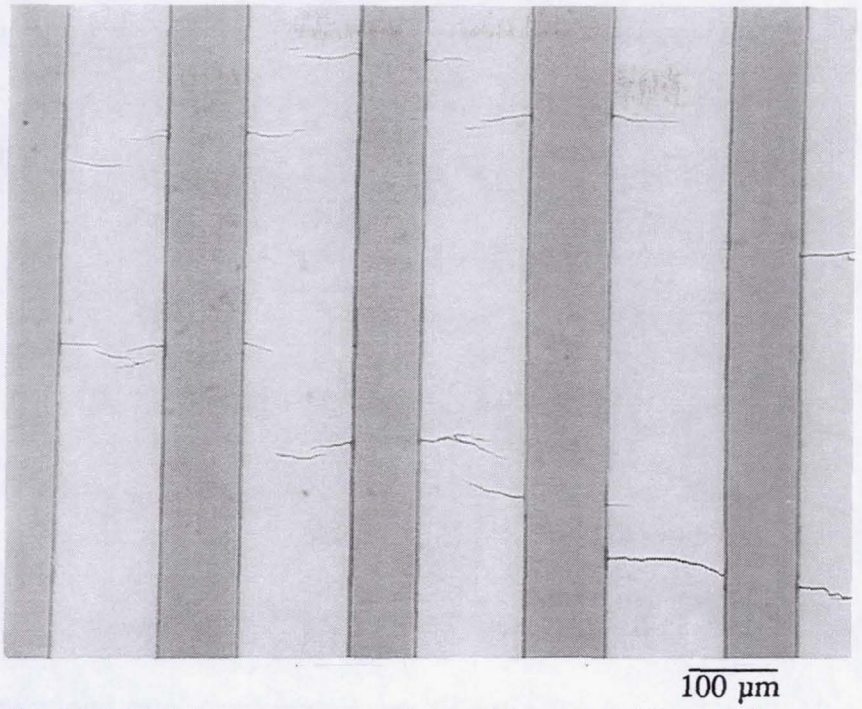

Figure 10. OP TMF damage progression at 90 percent N_f revealing considerable de-bonding and crack bridging evident in first fiber row.

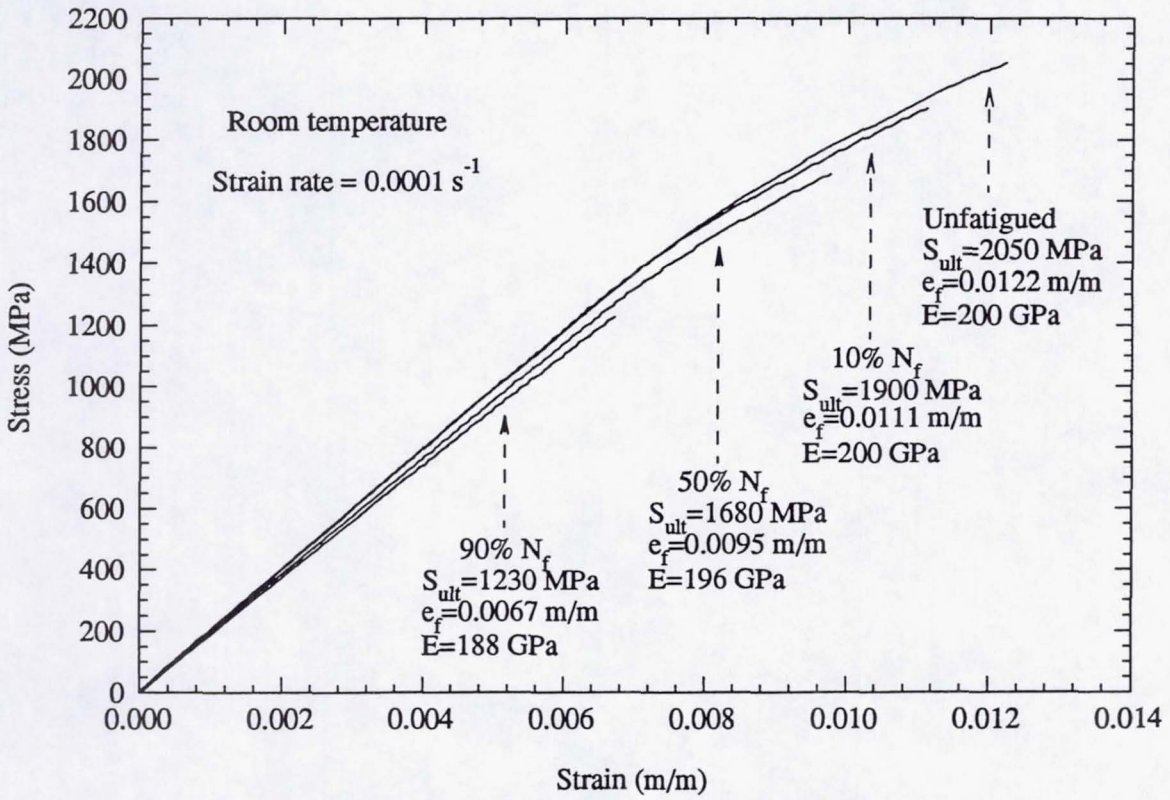

Figure 11. Room temperature tensile residual strength of SCS-6/Timetal 21S $[0]_4$ subjected to various percentages of OP TMF life with S_{max}= 1000 MPa.

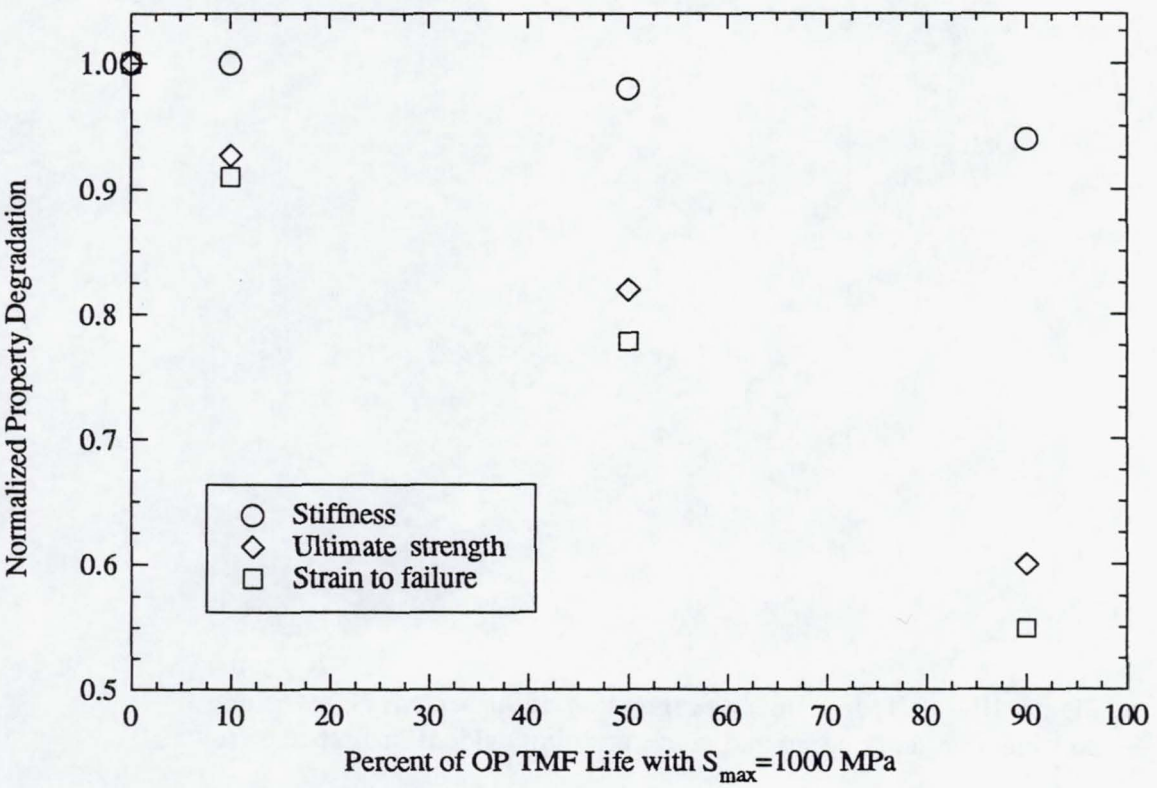

Figure 12. Normalized degradations of room temperature residual strength tensile properties at various percentages of OP TMF life ith S_{max}= 1000 MPa..

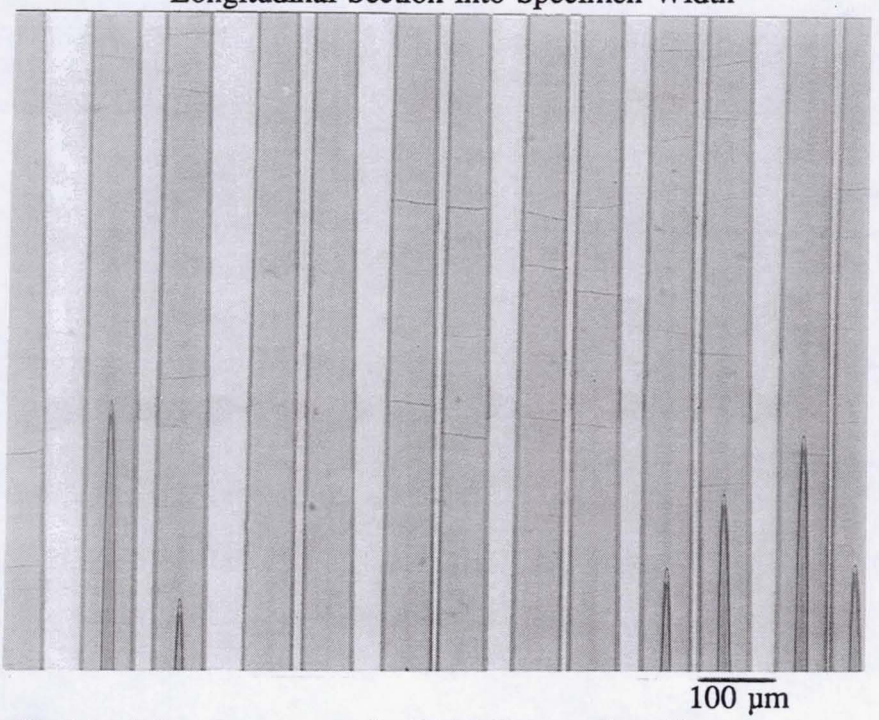

Figure 13. Initial damage state under IP TMF revealing fiber cracks.

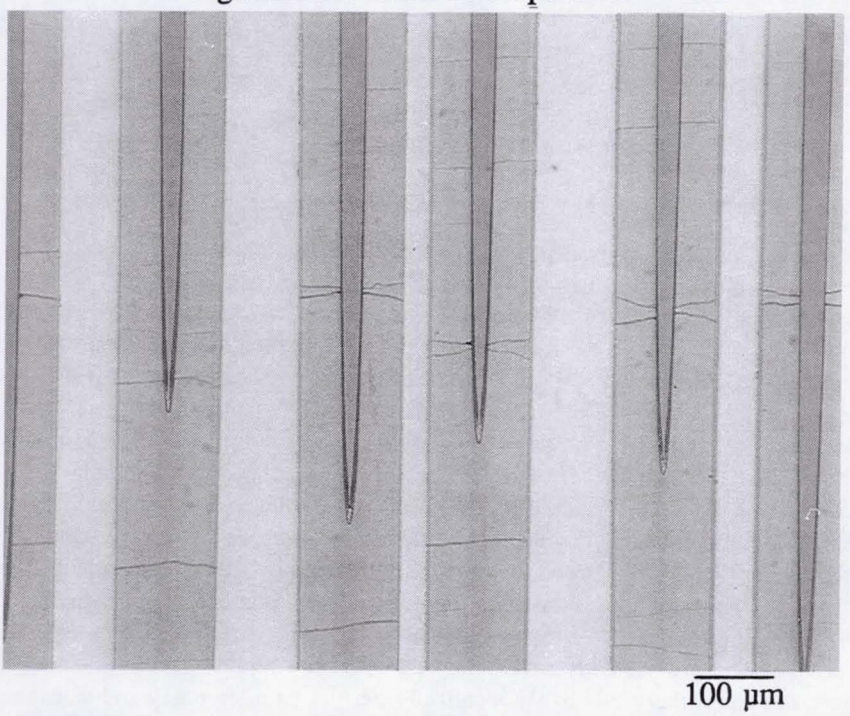

Figure 14. IP TMF damage progression at 50 percent N_f revealing "v-wedge" type fiber cracks as seen in the four right-most fibers.

REPORT DOCUMENTATION PAGE

Form Approved
OMB No. 0704-0188

1. AGENCY USE ONLY (*Leave blank*)	2. REPORT DATE	3. REPORT TYPE AND DATES COVERED
	November 1994	Final Contractor Report

4. TITLE AND SUBTITLE

Characterization of Damage Progression in SCS-6/Timetal 21S $[0]_4$ Under Thermomechanical Fatigue Loadings

5. FUNDING NUMBERS

WU–763–22–41
C–NAS3–27186

6. AUTHOR(S)

Michael G. Castelli

7. PERFORMING ORGANIZATION NAME(S) AND ADDRESS(ES)

NYMA, Inc.
Engineering Services Division
2001 Aerospace Parkway
Brook Park, Ohio 44142

8. PERFORMING ORGANIZATION REPORT NUMBER

E–9221

9. SPONSORING/MONITORING AGENCY NAME(S) AND ADDRESS(ES)

National Aeronautics and Space Administration
Lewis Research Center
Cleveland, Ohio 44135–3191

10. SPONSORING/MONITORING AGENCY REPORT NUMBER

NASA CR–195399

11. SUPPLEMENTARY NOTES

Prepared for the Symposium on Life Prediction Methodology for Titanium Matrix Composites sponsored by the American Society for Testing and Materials, Hilton Head, South Carolina, March 22–24, 1994. Project Manager, Rod Ellis, Structures Division, NASA Lewis Research Center, organization code 5220, (216) 433–3340.

12a. DISTRIBUTION/AVAILABILITY STATEMENT

Unclassified - Unlimited
Subject Category 24

12b. DISTRIBUTION CODE

13. ABSTRACT ***(Maximum 200 words)***

A detailed experimental investigation was performed at a single maximum cyclic stress (σ_{max}) level to physically characterize the progression of thermomechanical fatigue (TMF) damage in continuously reinforced [0°] SCS-6/Timetal 21S, a titanium matrix composite. In-phase (IP) and out-of-phase (OP) loadings were investigated at σ_{max} = 1000 MPa with a temperature cycle from 150 to 650°C. Damage progression, in terms of macroscopic property degradation, was experimentally quantified through an advanced TMF test methodology which incorporates explicit measurements of the isothermal static moduli at the TMF temperature extremes and the coefficient of thermal expansion (CTE) as functions of the TMF cycles. Detailed characterization of the physical damage progression at the microstructural level was performed by interrupting multiple TMF tests at various stages of mechanical property degradation and analyzing the microstructure through extensive destructive metallography. Further, the extent of damage was also quantified through residual static strength measurements. Results indicated that damage initiation occurred very early in cyclic life ($N < 0.1N_f$) for both the IP and OP TMF loadings. IP TMF damage was found to be dominated by fiber breakage with a physical damage progression in the microstructure which was difficult to quantify. OP TMF loadings produced matrix cracking exclusively associated with surface initiations. Here, damage progression was easily distinguished in terms of both the number of cracks and their relative inward progressions toward the outer fiber rows with increased cycling. The point at which the leading cracks reached the outer fiber rows (when localized fiber/matrix de-bonding and matrix crack bridging occurred) appeared to be reflected in the macroscopic property degradation curves.

14. SUBJECT TERMS

Metal matrix composites; Damage progression; Thermomechanical fatigue; Mechanical properties; Stiffness; Coefficient of thermal expansion

15. NUMBER OF PAGES

21

16. PRICE CODE

A03

17. SECURITY CLASSIFICATION OF REPORT	18. SECURITY CLASSIFICATION OF THIS PAGE	19. SECURITY CLASSIFICATION OF ABSTRACT	20. LIMITATION OF ABSTRACT
Unclassified	Unclassified	Unclassified	